nature nanotechnology

LETTERS

PUBLISHED ONLINE: 19 DECEMBER 2016 | DOI: 10.1038/NNANO.2016.277

Self-assembling DNA nanotubes to connect molecular landmarks

Abdul M. Mohammed[1], Petr Šulc[2], John Zenk[1] and Rebecca Schulman[1,3]*

Within cells, nanostructures are often organized using local assembly rules that produce long-range order[1,2]. Because these rules can take into account the cell's current structure and state, they can enable complexes, organelles or cytoskeletal structures to assemble around existing cellular components to form architectures[3–6]. Although many methods for self-assembling biomolecular nanostructures have been developed[7–11], few can be programmed to assemble structures whose form depends on the identity and organization of structures already present in the environment. Here, we demonstrate that DNA nanotubes can grow to connect pairs of molecular landmarks with different separation distances and relative orientations. DNA tile nanotubes nucleate at these landmarks and grow while their free ends diffuse. The nanotubes can then join end to end to form stable connections, with unconnected nanotubes selectively melted away. Connections form between landmark pairs separated by 1–10 μm in more than 75% of cases and can span a surface or three dimensions. This point-to-point assembly process illustrates how self-assembly kinetics can be designed to produce structures with a desired physical property rather than a specific shape.

In vivo, proteins and protein complexes often have precisely defined atomic structures. Larger assemblies, cells and tissues, while organized, can vary in shape, size or how their components are arranged without loss of function. For example, the arrangement of microtubules within the metaphase mitotic spindle varies from cell to cell, but microtubules consistently connect kinetochores to microtubule organizing centres[12–14]. Structure emerges as a consequence of assembly rules that govern both the interactions between the components that make up the final structure and the interactions between those components and their surroundings.

To investigate how to design such self-assembly processes, we considered the problem of self-assembling one-dimensional nanostructures that begin and end at molecular landmarks whose separation distance and orientation may vary (Fig. 1a). We proposed that connections between these landmarks could be formed using coupled polymer growth and rotational diffusion. Polymers could nucleate from the two landmarks and grow via monomer addition at their free ends, which would diffuse through solution during growth. When these ends meet, they could join, forming a connection (Fig. 1b). In our system, DNA nanotubes[15] form the connections and DNA origami[16] nanostructures that can template nanotube growth[17] act as the molecular landmarks, or seeds, termed A and B (Fig. 1c).

We tested point-to-point assembly using an assay in which connections formed between A and B seeds attached at random locations on a glass surface (Supplementary Section 2.3). Although point-to-point assembly should be able to form three-dimensional connections, this assay produced connections within a single image plane, making it possible to visualize the assembly process using fluorescence microscopy. Previous studies suggested that at 32 °C and 40 nM of tiles, nanotubes would grow efficiently from seeds but rarely nucleate homogeneously[17]. Under these conditions we confirmed that nanotubes grew from A or B seeds attached to the surface (Supplementary Fig. 9). We next studied how nanotubes grew and formed connections when both types of seed were present on the surface. Nanotube interconnects formed between many A and B seeds (Fig. 2a and Supplementary Fig. 46). No visible kinks in connected structures, which conceivably may have been created by joining[18,19], were observed.

To verify that nanotube connections assembled via the designed process of nucleation from seeds, growth and joining, we captured time-lapse fluorescence microscopy movies of five nanotube connection processes (Supplementary Section 6.5). Nanotubes grew from both seed types and usually increased in length gradually, consistent with growth by monomer addition. Connections formed soon after their ends were observed near one another (Supplementary Movie 1) and were stable for at least 10 h. In one movie, a free nanotube joined a seeded nanotube, resulting in a sudden, large increase in the seeded nanotube's length (Supplementary Fig. 50).

To measure yields, we characterized how often connections formed between isolated pairs of A and B seeds. A pair was deemed isolated if A and B were separated by interlandmark distance d and no other B seed was within distance $1.5d$ of seed A and vice versa (Supplementary Fig. 12). Because the ends of longer nanotubes must explore more volume to find one another than the ends of shorter ones, yields should decrease with interlandmark distance. Longer ends also explore space more slowly because rotational and translational diffusion rates slow with polymer length[20].

After 10, 20, 30 and 40 h, more than 80% of connections with interlandmark distances below a threshold formed, but yields were poor at longer distances. This threshold increased from 1 μm at 10 h to 5 μm at 40 h (Fig. 2c and Supplementary Section 3.1). A total of 87.5% of connected nanotubes after 30 h were direct, that is, they had contour lengths less than 1.5 times the interlandmark distance, but a few had contour lengths as large as 3.75 times this distance (Fig. 2d and Supplementary Fig. 14). Connections failed to form primarily because the growing nanotubes were not yet long enough to reach one another: for example, after 30 h, 88% of the unconnected pairs had nanotubes too short to reach one another (Fig. 2e). Diffusion was therefore generally fast enough with respect to growth to allow nanotube ends to connect soon after they were able to.

To form longer connections, we allowed point-to-point assembly to proceed over 70 h. We replenished the tiles in the surrounding solution twice using buffer exchange to ensure monomer depletion did not affect nanotube growth rates (Supplementary Section 3.1).

[1]Chemical and Biomolecular Engineering, Johns Hopkins University, Baltimore, Maryland 21218, USA. [2]Center for Studies in Physics and Biology, The Rockefeller University, New York, New York 10065, USA. [3]Computer Science, Johns Hopkins University, Baltimore, Maryland 21218, USA. *e-mail: rschulm3@jhu.edu

© 2016 Macmillan Publishers Limited, part of Springer Nature. All rights reserved.

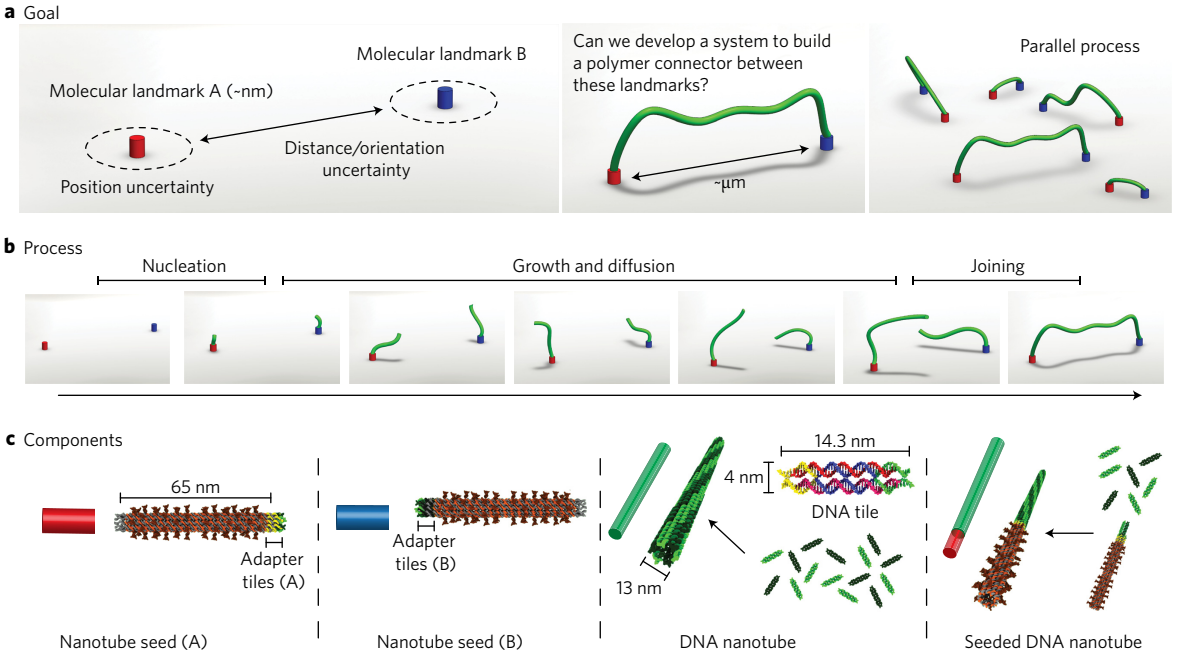

Figure 1 | Scheme for assembling interconnects between fixed molecular landmarks and the DNA nanostructures used within the assembly process. **a**, The goal of point-to-point assembly is to reliably build polymer connections between molecular landmarks whose relative orientations and separation distances can vary. Here, we considered molecular landmarks with sizes on the order of nanometres that are separated by from 1 to 10 μm. **b**, In point-to-point assembly, polymers nucleate at the molecular landmarks and grow from their free ends via monomer addition. Polymer ends diffuse during growth and if they meet, join to form a stable connection. **c**, DNA tile nanotubes serve as polymer connectors and DNA nanotube seeds (A and B) serve as molecular landmarks to be connected. A and B seeds are DNA origami nanostructures with different 'adapter tiles' that template nanotube growth at opposite ends. DNA tiles hybridize to seeds and nanotubes via complementary single-stranded DNA 'sticky ends' (see Supplementary Section 1 for sequences and details).

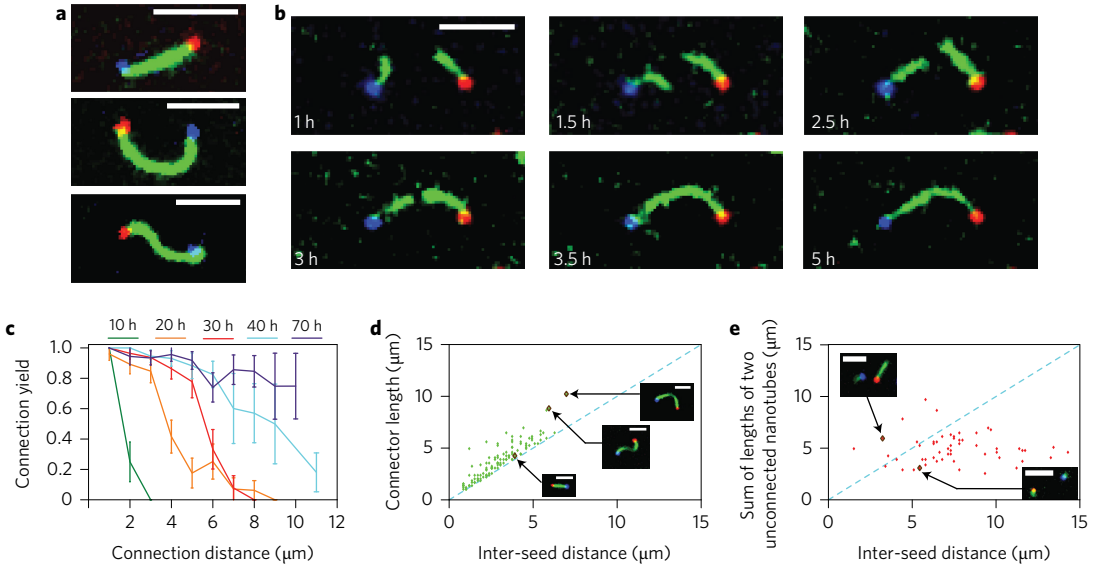

Figure 2 | DNA nanotubes connecting molecular landmarks. **a**, Multicolour fluorescence images showing DNA nanotubes connecting two nanotube seeds (A and B). DNA nanotubes are labelled with Cy3 dye (green), seed A with ATTO647N dye (red) and seed B with ATTO488 dye (blue). Scale bars, 5 μm. **b**, Time-lapse multicolour fluorescence microscopy confirms DNA nanotube connections form via the process in Fig. 1b. Six still frames over 5 h are shown. Nanotube connection takes place at ~3.5 h. Scale bar, 5 μm. **c**, Interconnection yields as a function of inter-seed distance for different assembly times. Error bars are generated via bootstrapping and indicate one standard deviation. $N = 75$, 190, 178, 163 and 157 for 10, 20, 30, 40 and 70 h, respectively. During the 70 h process, two iterations of buffer exchange replace depleted monomers. **d**, Scatter plot relating inter-seed distance and the lengths of successful nanotube connections after 30 h of assembly time. Points closer to the blue diagonal line are 'straighter' connections, while those further away are much longer than the distance between seeds. Insets: images of nanotube connections corresponding to the respective green dots. Scale bar, 5 μm. **e**, Scatter plot comparing the sum of the lengths of the unconnected nanotubes that grew from the two landmarks with inter-landmark distance after 30 h of assembly time. Points below the blue dashed line show nanotube pairs not long enough to reach one another. Insets: images of unsuccessful nanotube connections corresponding to the respective red dots. Scale bars, 5 μm.

© 2016 Macmillan Publishers Limited, part of Springer Nature. All rights reserved.

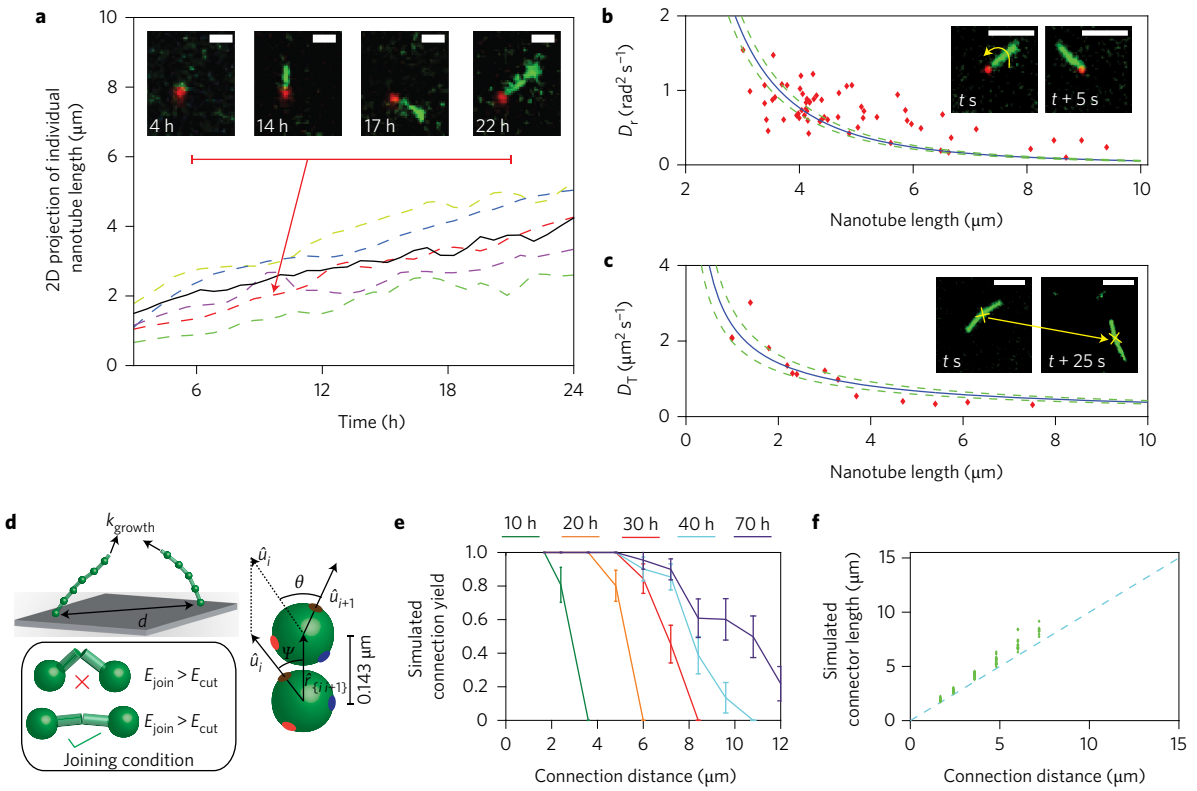

Figure 3 | Model calibrated using measured nanotube growth rates, and rotational and translational diffusion constants that reproduces the connection yields from experiment. a, Increases in length over time of five randomly selected seeded nanotubes (shown in dotted lines) as determined from fluorescence micrographs. The black trend line is the average nanotube length calculated from 35 nanotubes. Two-dimensional projection of nanotube length was used as an estimate for nanotube length. Insets: an example DNA nanotube (red dotted line) at different points during growth. Scale bars, 2 μm. **b**, Measured rotational diffusion coefficients D_r (red) of individual seeded nanotubes as a function of nanotube length (Supplementary Section 3.4). Blue line: fit of an equation relating D_r of a rod-shaped particle as a function of rod length. Dashed green lines indicate 95% asymptotic confidence intervals. Insets: example frames from one microscopy movie used to measure D_r; rotation was measured about the seed. Scale bars, 5 μm. **c**, Measured translational diffusion coefficients (red) of individual seeded nanotubes in two-dimensional confinement as a function of nanotube length (Supplementary Section 3.5). Blue line: fit of an equation relating D_T of a rod-shaped particle as a function of rod length. Dashed green lines indicate 95% asymptotic confidence intervals. Insets: selected frames from an example movie used to measure D_T of a seeded DNA nanotube moving in two-dimensional confinement. Scale bars, 5 μm. **d**, Schematic of a coarse-grained molecular dynamics model of point-to-point assembly. Nanotubes are represented as chains of beads with mean distance between adjacent beads corresponding to 0.143 μm of nanotube. The interaction energy between neighbouring beads depends on their distance apart ($\hat{r}_{(i\,i+1)}$) and orientations (given in terms of angles θ and ψ) and is parameterized to reproduce the measured persistence length of 8.7 ± 0.5 μm. The chains grow by adding new beads at rate k_{growth}. The nanotubes are considered joined if the interaction energy E_{join}, which depends on the distance and mutual orientation of the last two beads of the respective chains, is below the threshold E_{cut}. D_r and D_T, whose fits are shown in Fig. 3b,c, were used to fit the timescales of the dynamics in the model. For details see Supplementary Section 4. **e**, Interconnection yields as a function of time predicted by simulation (**d**) for a persistence length, diffusion rates and joining rates close to those measured experimentally; varying parameters can significantly change the predicted yields (Supplementary Section 4.3). Error bars represent one standard deviation, generated via bootstrapping. **f**, Scatter plot relating the lengths of nanotube connections found in simulation and the distance between seeds after 30 simulated hours of assembly using the same parameters as in **e**. Blue dashed line: shortest possible connector length for each connection distance.

Nanotube connections between pairs as far as 10 μm apart formed with >70% yield (Fig. 2c). Only a few nanotubes in isolated pairs were too short to make a connection (11%, $n = 2$) (Supplementary Fig. 49). However, 39% ($n = 7$) had one nanotube that could not rotate freely, possibly because multiple biotin–neutravidin bonds could form between the seed and the surface, limiting rotation, or because the polyethylene glycol on the passivated surface and the seed's excess scaffold entangled, and 22% ($n = 4$) were partially stuck to the surface. There was no visible reason for the failed connection of the remaining 28% ($n = 5$).

To better understand point-to-point assembly, we built a coarse-grained model of the process that combines established methods for simulating DNA tile nanotube growth[17,21,22] and worm-like chain polymer dynamics (Supplementary Section 4). Nanotubes are modelled as chains of beads separated by springs[23]. Growth occurs through stochastic addition of beads to the chain, while joining is allowed when chain ends are sufficiently close and the bending energy based on the orientation of the joining beads is below a specified threshold (Fig. 3d and Supplementary Section 4.1).

We calibrated the model to reproduce the nanotube growth and diffusion rates in our experiments. Time-lapse fluorescence microscopy following individual nanotubes (Fig. 3a) showed that nanotubes grew at a constant rate (0.11 ± 0.01 μm h^{-1}) over 24 h. This rate is consistent with a measured forward rate constant[21] of tile hybridization of 6×10^5 M^{-1} s^{-1} and an energy[17] of DNA tile attachment of −10.9 kcal mol^{-1} at 32 °C. A joining rate of $2.9 \pm 1.7 \times 10^6$ M^{-1} s^{-1} was measured by observing the rate at which seeded nanotubes joined in bulk (Supplementary Section 3.7). To measure the length-dependent nanotube rotational diffusion rate, we tracked nanotube angular motion parallel to the x–y plane (Fig. 3b and Supplementary Section 3.4). We similarly measured the length-dependent translational diffusion rate by following

© 2016 Macmillan Publishers Limited, part of Springer Nature. All rights reserved.

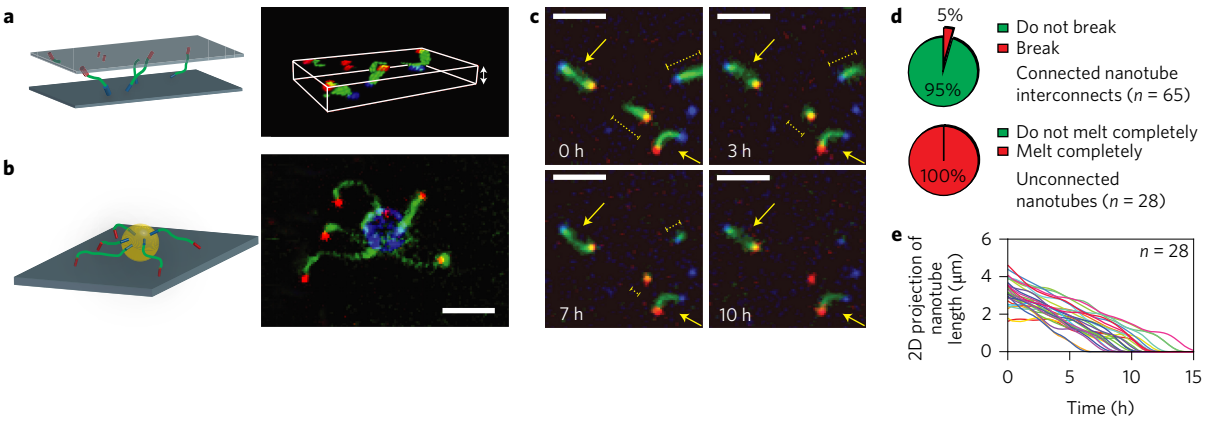

Figure 4 | Assembly of DNA nanotube interconnects in three dimensions and selective melting of unconnected nanotubes. a, Left: perspective representation of DNA nanotube interconnects between type A seeds attached to the top glass surface and type B seeds attached to the bottom glass surface. Right: three-dimensional confocal micrograph showing multiple nanotube connections (green, Cy3 dye) spanning the two parallel glass surfaces connecting A seeds (red, ATTO647N dye) and B seeds (blue, ATTO488 dye). The two glass surfaces shown are separated by 3.5 μm. **b**, Left: perspective representation of DNA nanotube interconnects between type A seeds attached to a glass surface and type B seeds attached to a bead. Right: three-colour fluorescence image showing multiple nanotube connections (green, Cy3 dye) between seeds (blue, ATTO488 dye) on a 3 μm bead and seeds (red, ATTO647N dye) on the glass surface. Scale bar, 5 μm. **c**, Multicolour fluorescence micrographs of the same structures over 10 h showing preferential melting of unconnected DNA nanotubes after removal of free monomers. Arrows point to connected nanotubes and dotted line segments indicate lengths of unconnected nanotubes. Scale bars, 5 μm. **d**, Percentages of connected nanotubes that break within 15 h after free monomers are removed (top) and proportion of unconnected nanotubes that melt completely in the same environment (bottom). **e**, Decreases in length of individual unconnected nanotubes over time after free monomers are removed, as determined by fluorescence microscopy.

nanotubes as they freely diffused in two-dimensional confinement (Fig. 3c and Supplementary Section 3.5). Analysis of similar movies showed nanotubes have a persistence length of 8.7 ± 0.5 μm (Supplementary Section 3.6), in agreement with previous measurements under different conditions as well as theoretical estimates[15,24].

We used this model to understand how different physical parameters control the outcome of point-to-point assembly. For a timescale and joining threshold energies that correspond reasonably with measured diffusion rates, joining rates and nanotube persistence length, the model predicted yields and nanotube contour lengths similar to those observed experimentally (Fig. 3e,f). Slower growth and longer assembly times improve connection yields, particularly at larger interlandmark distances (Supplementary Figs 34 and 35), but the influence of other factors was more complex. For example, altering the threshold energy at which joining can occur can dramatically affect connection yields, suggesting that the molecular details of end joining are key to the success of the process (Supplementary Figs 33 and 34). Flexible polymers (with persistence lengths an order of magnitude smaller than interlandmark distance) did not connect as reliably and the connections that formed were usually much longer than the interlandmark distance and took a long time to grow (Supplementary Fig. 36). Rigid polymers (with persistence lengths an order of magnitude or more larger than interlandmark distance) also formed connections poorly, because once they grow even slightly longer than the interlandmark distance, the bending required for the ends to meet and join is strongly disfavoured (Supplementary Figs 37 and 38). Polymers with persistence lengths comparable to the length scales of the interlandmark distances, like DNA nanotubes connecting over several micrometres, connected best (Supplementary Fig. 35). Qualitative arguments based on geometry relating the probability distributions of polymer end locations to connection yields also support these trends (Supplementary Section 5.2).

The most consistent difference between simulations and experiment was that short connections formed at 100% yields in simulations but not in experiments (Figs 2c and 3e). We hypothesized that the inability of some nanotubes to diffuse freely might make the connection of some pairs difficult or impossible. We characterized the rotational motion of 70 nanotubes in the x–y plane over 24 h and found the motion of 90% of nanotubes to be restricted (Supplementary Section 3.2), with 50% of nanotubes exploring less than 70% of the available angles. We incorporated this effect into simulations by restricting the rotation of the first bead of each chain only through the angular range accessible by a randomly chosen nanotube whose motion we measured. These simulations predicted yields at shorter distances similar to those observed experimentally (80–90%), but yields for longer interlandmark distances were largely unaffected by rotational restriction (Supplementary Section 4.5). These results reflect the disparate effects of restricted diffusion. Restricted rotational diffusion often makes connection more difficult, but some types of restriction can actually enhance the probability of connection by orienting nanotube ends towards one another (Supplementary Section 5.3). At longer interlandmark distances these effects can largely balance. However, a small fraction of nanotubes may be oriented away from each other in a way that makes connection very difficult, and this effect is particularly apparent at short interlandmark distances, where nanotubes would otherwise virtually always form connections.

To confirm that point-to-point assembly can create three-dimensional connections between landmarks on different surfaces, we attached A seeds to one passivated glass slide and B seeds to another and assembled the slides into a fluid chamber filled with tiles. Three-dimensional confocal fluorescence micrographs showed nanotube connections (Fig. 4a, Supplementary Fig. 51 and Supplementary Movie 2). To explore point-to-point assembly in a heterogeneous environment, we attached B seeds to 3-μm-diameter polystyrene beads and deposited the beads into glass dishes where A seeds were attached at random locations across the surface. Connections formed reliably between the A and B seeds (Fig. 4b, Supplementary Fig. 52 and Supplementary Movie 3).

Every monomer in a DNA nanotube connector is attached to four other monomers by four sticky end bonds. In contrast, unconnected nanotubes have at least one free end where monomers are connected to just two neighbours (Supplementary Section 3.8).

© 2016 Macmillan Publishers Limited, part of Springer Nature. All rights reserved.

The first steps in the melting of connected nanotubes should therefore be detachments of monomers by four sticky end bonds, whereas unconnected nanotubes could begin melting by detachments of monomers by just two bonds. There could thus be an energy barrier to the melting of connected nanotubes, which would make it possible to disassemble unconnected nanotubes without affecting connected ones. After assembling nanotube connections, we removed the free tiles from solution using buffer exchange so that nanotubes could melt. After 15 h, 100% ($n = 28$) of the unconnected nanotubes we tracked melted away, while 95% of connected nanotubes remained intact (Fig. 4c–e and Supplementary Movie 4). The rates of connected and unconnected nanotube melting measured at different temperatures are consistent with the existence of an energy barrier to the melting of connected nanotubes (Supplementary Section 3.8).

Point-to-point assembly demonstrates how nanostructures can be self-assembled so that their shape and position are coordinated both by the assembling molecules and different existing nanostructures and their locations. The use of DNA and the origami technique means that different sets of connectors and landmarks made from different sequences or multivalent landmark sites could be used to form more complex patterns. Such systems could also be controlled by DNA-based circuits[25,26]. Functionalization of connectors with metals[27,28], lipids[29] and other molecules could also make it possible to use this technique to build circuits or channels that connect pre-existing terminals. More generally, point-to-point assembly demonstrates that self-assembly processes can be designed to stop when an assembly attains a particular function or property, rather than when a predefined target structure has formed. Non-functional structures can also be removed while functional structures remain intact. Such a function-driven approach could be a route to self-assembling complex devices reliably in a range of environments.

Data availability

The data that support the findings of this study are available from the corresponding author upon reasonable request.

Received 1 September 2015; accepted 16 November 2016; published online 19 December 2016

References

1. Fletcher, D. A. & Mullins, D. Cell mechanics and the cytoskeleton. *Nature* **463,** 485–492 (2010).
2. Misteli, T. The concept of self-organization in cellular architecture. *J. Cell Biol.* **155,** 181–185 (2001).
3. Vignaud, T., Blanchoin, L. & Thery, M. Directed cytoskeleton self-organization. *Trends Cell Biol.* **22,** 671–682 (2012).
4. Wang, N., Tytell, J. D. & Ingber, D. E. Mechanotransduction at a distance: mechanically coupling the extracellular matrix with the nucleus. *Nat. Rev. Mol. Cell Biol.* **10,** 75–82 (2009).
5. Greenfield, D. *et al.* Self-organization of the *Escherichia coli* chemotaxis network imaged with super-resolution light microscopy. *PLoS Biol.* **7,** e1000137 (2009).
6. Alberts, B. *et al. Molecular Biology of the Cell* 4th edn (Garland Science, 2002).
7. Hartgerink, J. D., Beniash, E. & Stupp, S. I. Self-assembly and mineralization of peptide-amphiphile nanofibers. *Science* **294,** 1684–1688 (2001).
8. Percec, V. *et al.* Self-assembly of janus dendrimers into uniform dendrimersomes and other complex architectures. *Science* **328,** 1009–1014 (2010).
9. Douglas, S. M. *et al.* Self-assembly of DNA into nanoscale three-dimensional shapes. *Nature* **459,** 414–418 (2009).
10. Barish, R. D., Schulman, R., Rothemund, P. W. K. & Winfree, E. An information-bearing seed for nucleating algorithmic self-assembly. *Proc. Natl Acad. Sci. USA* **106,** 6054–6059 (2009).
11. Wei, B., Dai, M. J. & Yin, P. Complex shapes self-assembled from single-stranded DNA tiles. *Nature* **485,** 623–626 (2012).
12. Dinarina, A. *et al.* Chromatin shapes the mitotic spindle. *Cell* **138,** 502–513 (2009).
13. Gadde, S. & Heald, R. Mechanisms and molecules of the mitotic spindle. *Curr. Biol.* **14,** R797–R805 (2004).
14. Helmke, K. J., Heald, R. & Wilbur, J. D. Interplay between spindle architecture and function. *Int. Rev. Cell Mol. Biol.* **306,** 83–125 (2013).
15. Rothemund, P. W. K. *et al.* Design and characterization of programmable DNA nanotubes. *J. Am. Chem. Soc.* **126,** 16344–16352 (2004).
16. Rothemund, P. W. K. Folding DNA to create nanoscale shapes and patterns. *Nature* **440,** 297–302 (2006).
17. Mohammed, A. M. & Schulman, R. Directing self-assembly of DNA nanotubes using programmable seeds. *Nano Lett.* **13,** 4006–4013 (2013).
18. Rothwell, S. W., Grasser, W. A. & Murphy, D. B. End-to-end annealing of microtubules *in vitro*. *J. Cell Biol.* **102,** 619–627 (1986).
19. Ekani-Nkodo, A., Kumar, A. & Fygenson, D. K. Joining and scission in the self-assembly of nanotubes from DNA tiles. *Phys. Rev. Lett.* **93,** 268301 (2004).
20. Doi, M. & Edwards, S. F. *The Theory of Polymer Dynamics* (Clarendon, 1988).
21. Hariadi, R. F., Yurke, B. & Winfree, E. Thermodynamics and kinetics of DNA nanotube polymerization from single-filament measurements. *Chem. Sci.* **6,** 2252–2267 (2015).
22. Mardanlou, V. *et al.* A coarse-grained model of DNA nanotube population growth. in *DNA Computing and Molecular Programming* (eds Rondelez, Y. & Woods, D.) 135–147 (2016).
23. Brackley, C. A., Morozov, A. N. & Marenduzzo, D. Models for twistable elastic polymers in Brownian dynamics, and their implementation for LAMMPS. *J. Chem. Phys.* **140,** 135103 (2014).
24. Schiffels, D., Liedl, T. & Fygenson, D. K. Nanoscale structure and microscale stiffness of DNA nanotubes. *ACS Nano* **7,** 6700–6710 (2013).
25. Zhang, D., Hariadi, R. F., Choi, H. & Winfree, E. Integrating DNA strand-displacement circuitry with DNA tile self-assembly. *Nat. Commun.* **4,** 1965 (2013).
26. Montagne, K., Plasson, R., Sakai, Y., Fujii, T. & Rondelez, Y. Programming an *in vitro* DNA oscillator using a molecular networking strategy. *Mol. Syst. Biol.* **7,** 466 (2011).
27. Tan, S., Campolongo, M., Luo, D. & Cheng, W. Building plasmonic nanostructures with DNA. *Nat. Nanotech.* **6,** 268–276 (2011).
28. Knudsen, J. B. *et al.* Routing of individual polymers in designed patterns. *Nat. Nanotech.* **10,** 892–898 (2015).
29. Wilner, O. I. & Willner, I. Functionalized DNA nanostructures. *Chem. Rev.* **112,** 2528–2556 (2012).

Acknowledgements

The authors thank D. Fygenson, M. Bevan, D. Gracias, E. Winfree, D. Agrawal, S. Schaffter and E. Franco for discussions and advice on the manuscript, J. Liphardt for the use of equipment and advice, and J. Fern, E. Pryce, R. Zuckermann and C. Ajo-Franklin for technical advice. This research has been supported by DOE grant DE-SC0010595, which provided money for materials, supplies and computing time, NSF CAREER award 125387, and the Miller Institute for Basic Science. P.Š. is supported by a grant from the Simons Foundation. Preliminary work related to this project at the Molecular Foundry was supported by the Office of Science, Office of Basic Energy Sciences, of the US Department of Energy, under contract no. DE-AC02-05CH11231.

Author contributions

A.M.M. and R.S. designed the experiments and carried out the experimental analysis. A.M.M. conducted the experiments. P.Š. and R.S. designed the simulations. P.Š. and J.Z. developed simulations and analysed simulation results. All the authors discussed the results and wrote the manuscript.

Additional information

Supplementary information is available in the online version of the paper. Reprints and permissions information is available online at www.nature.com/reprints. Correspondence and requests for materials should be addressed to R.S.

Competing financial interests

The authors declare no competing financial interests.

© 2016 Macmillan Publishers Limited, part of Springer Nature. All rights reserved.